Nodal Numerical Modeling of Submerged Helium Injection in a Cryogenic Propellant Tank

Michael R. Baldwin*
GeoControl Systems/Jacobs Space Exploration Group, Huntsville, AL, 35812, USA

and

Alok K. Majumdar† Andre C. LeClair‡
NASA Marshall Space Flight Center, Huntsville, AL, 35812, USA

Subcooling of cryogenic propellant by helium injection is one of the most effective methods for suppressing bulk boiling and keeping subcooled propellant conditions for pre-launch, launch, and post-launch pressurization applications. For tank pressurization, submerged helium injection can substantially reduce helium consumption by infusing gaseous propellant into the tank ullage. This paper presents a mathematical model of the helium bubbling process in liquid oxygen to estimate the amount of oxygen vapor absorbed by the rising helium bubbles and the amount of subcooling of liquid oxygen due to evaporative heat and mass transfer. This mathematical model was incorporated in a simulation model of tank pressurization built with Generalized Fluid System Simulation Program (GFSSP), a general-purpose flow network code developed at NASA/Marshall Space Flight Center. The numerical predictions of subcooling have been compared with the experimental data of Cho et al. which investigated the propellant subcooling effect as a function of system pressure, helium injection temperature, and flowrate for a non-drained submerged injection system. The numerical predictions of helium consumption have been compared with the test data from a NASA Centaur test vehicle which included both direct and submerged injection with draining of propellants. The numerical model developed with GFSSP has been validated against two sets of experimental data and has been shown to predict both propellant subcooling and helium consumption to within 30% in most cases. The test data used for the model validation were taken in 1-g, but the mass diffusion model was developed to be applied in both 1-g and micro-g environments.

Nomenclature

C_p = isobaric specific heat [kJ/kg/K]
h = enthalpy [kJ/kg]
h_g = saturated vapor enthalpy [kJ/kg]
h_{fg} = enthalpy of vaporization [kJ/kg]
m_{LOx} = propellant mass [kg]
m_u = ullage mass [kg]
$\dot{m}_{drain}$ = propellant drain rate [kg/s]
$\dot{m}_{vent}$ = ullage vent rate [kg/s]
$\dot{m}_{He}$ = inlet helium injection rate [kg/s]

* Thermal Analysist for Liquid Propulsion Systems, NASA Marshall Space Flight Center.

† Thermal Analysist for Liquid Propulsion Systems, NASA Marshall Space Flight Center.

‡ Thermal Analysist for Liquid Propulsion Systems, NASA Marshall Space Flight Center.

$\dot{m}_{ev}$ = boil-off mass transfer rate [kg/s]
$\dot{m}_{O_2}$ = diffusional mass transfer rate [kg/s]
P_{O_2} = partial pressure of oxygen [kPa]
P_{He} = partial pressure of helium [kPa]
P_u = ullage pressure [kPa]
$\dot{Q}$ = ullage-to-propellant heat transfer rate [W]
$\dot{Q}_{leak}$ = heat leak [W]
R = specific gas constant [kJ/K/kmol]
$T_{initial}$ = propellant temperature at beginning of simulation [K]
$T_{He,in}$ = injected helium temperature [K]
T_{final} = propellant temperature at end of simulation [K]
T_{prp} = propellant temperature [K]
T_{sat} = saturation temperature [K]
t = time [s]
$\dot{V}$ = volumetric flowrate [m^3/s]

Greek Letters
$\Delta\dot{h}$ = change in enthalpy rate [kW/kg]
ΔT_{sub} = propellant subcooling [K]
Δt = time step [s]
ΔV = change in volume [m^3]
ε_{cons} = error between simulated and experimental helium consumption [-]
ε_{sub} = error between simulated and experimental propellant subcooling [-]
ρ = density [kg/m^3]

Subscripts
cons = consumption
ev = evaporation
exp = experiment
f = fluid phase
g = gas phase
He = helium
LOx = liquid oxygen
O_2 = oxygen
prp = propellant
sat = saturation
sim = simulation
sub = subcooling
u = ullage

I. Introduction and Background

Pressurizing a cryogenic tank before and during engine firing is traditionally performed by injecting pressurant gas directly into the ullage. The idea of injecting the pressurant gas into the liquid propellant as a method of pressurization was investigated in the 1960s but received little attention thereafter. The past two decades have seen a small revival in the level of interest of this submerged injection system, presumably from the benefits such a system offers. A submerged injection system harnesses the mass transfer phenomena between the pressurant gas and liquid propellant, which results in propellant subcooling. This helps to avoid liquid propellant boiling in the engine transfer lines and turbo-pump cavitation. The evaporation of the propellant that takes place during this process helps to pressurize the ullage, lessening the amount of pressurant gas required during the pressurization process. The amount of pressurant savings is substantial enough that the possibility of reducing the size or number of pressurant supply tanks on board the flight vehicle is practical. Finally, the warm pressurant gas undergoes heat transfer with the surrounding liquid propellant as the gas bubbles rise to the ullage. The cooled gas entering the ullage lowers the risk of ullage collapse.

Submerged injection test data were found from a series of runs on a Centaur test vehicle in 1968. These tests include a brief pre-pressurization and hold period, followed by a tank drain. The pressurant and propellant used were helium and oxygen, respectively. Initial ullage pressure and injection temperature were varied throughout the test cases. Within the past two decades, a few academic groups have researched the effects of submerged injection on propellant subcooling. The systems investigated here are helium-oxygen systems, do not include liquid propellant draining, and focus solely on the pressurant-propellant heat and mass transfer. From an analysis standpoint, both the heat and the mass transfer can either be modeled as instantaneous or non-instantaneous. An instantaneous heat and mass transfer approach is the simplest and assumes instant thermodynamic equilibrium between the injected gas and the surrounding liquid propellant. A non-instantaneous approach considers more complicated phenomena such as bubble departure and growth, and the transient effects of heat and mass transfer on the rising bubbles. The work referred to in the present study [1-2] has demonstrated that an instantaneous mass transfer approach is more than sufficient to model the mass transfer physics. This is possible with a diffuser that released bubbles with smaller volume-to-area ratios. Noticeable discrepancy is present between the two heat transfer approaches.

The present work uses an instantaneous heat and mass transfer model in NASA's GFSSP to predict the amount of propellant subcooling and helium usage during pressurization. The mathematical formulation for these processes does not depend on gravity and thus can be applied to any gravitational environment. For submerged injection systems, the effect of gravity will impact the buoyant force on the bubbles. Higher-g environments will decrease the residence time of the bubbles in the liquid propellant, allowing for more error in the instantaneous models; however, the opposite is true for lower-g environments. This apparent drawback can be mitigated through proper submerged diffuser design such that the significance of the bubble residence time in the liquid is greatly reduced. With its microgravity capability, the model is applicable for analyzing post-launch pressurizations including low earth orbit (LEO) operations, depot propellant transfer operations, trans-lunar injection (TLI) burn and lunar orbit burn.

This work aims to assess the capability of GFSSP to simulate tank pressurization utilizing a submerged injection system. Simulation results will be compared to the test data of a Centaur test vehicle and of some apparatus found in the literature containing helium-oxygen submerged injection systems. A secondary objective of this work is to evaluate the sufficiency of an instantaneous heat transfer model and to determine the need, if any, for a non-instantaneous heat transfer approach. Finally, the results of the submerged pressurization systems will be compared to data obtained from traditional direct ullage injection pressurization systems at similar operating conditions. Several direct ullage injection test cases are also included in the Centaur report. It is desired to ascertain the advantages of utilizing a submerged injection pressurization system and to understand their effects and practicality, should a new cryogenic tank pressurization system be needed in the future.

II. Mathematical Approach

GFSSP contains a direct ullage tank pressurization model that was validated several years ago with data from the FASTRAC engine tests. The physical model contains a single ullage node and a single liquid propellant node, in addition to a pressurant gas supply node and a draining branch to the engine boundary node. A pseudo-boundary node separates the ullage and liquid propellant nodes, preventing the two-phase mixing that would otherwise occur in a homogeneous code. The tank pressurization model allows for custom tank design and customizable natural convection heat transfer correlations between the ullage and liquid as well as between the ullage and tank wall. The tank pressurization model also automatically tracks the volume changes in the ullage and liquid propellant nodes and the change in gravitational pressure head as the tank drains. An optional user subroutine can model mass transfer from liquid to ullage via boil-off. This mass transfer rate at the liquid-ullage interface is approximated as:

$$\dot{m}_{\mathrm{ev}} = \frac{\dot{Q}}{h_{\mathrm{fg}} + C_{\mathrm{p}}(T_{\mathrm{sat}} - T_{\mathrm{prp}})} \tag{1}$$

The mathematical model for a submerged injection system is now presented. The present work includes the mathematics discussed above but also contains a set of equations to model the mass and heat transfer from the liquid propellent to the rising pressurant bubbles. From here on, the pressurant gas will be referred to as helium for simplicity. The following model assumes instantaneous heat and mass transfer, and so thermodynamic equilibrium is assumed throughout the entire process. First, the heat transfer is discussed. The helium enters the liquid near the bottom of the tank at a specified temperature, always warmer than that of the liquid propellant. The bubble is assumed to cool instantly to the temperature of the surrounding propellant, supplying the propellant with energy equal to the change in helium bubble enthalpy,

$$\Delta\dot{h} = \dot{m}_{\mathrm{He}} C_{\mathrm{p,He}} \left(T_{\mathrm{He,in}} - T_{\mathrm{prp}}\right) \tag{2}$$

Next, the mass transfer is discussed. According to Fick's Law, the helium gas injected into the propellant creates an oxygen concentration gradient across the helium bubble interface. Some of the oxygen atoms within the oxygen-rich propellant evaporate and diffuse into the helium bubbles to reach a state of concentration equilibrium. The equilibrium state is when the partial pressure of oxygen in the bubble is balanced by the oxygen saturation pressure at the liquid propellant temperature. The instantaneous diffusion model incorporated here assumes this condition is immediately reached. The bubble, now containing both gaseous oxygen and helium, follows Dalton's Law of Partial Pressure:

$$P_{\mathrm{u}} = P_{\mathrm{O_2}} + P_{\mathrm{He}} \tag{3}$$

where the total pressure of the rising bubble is equal to the ullage pressure when the bubble merges with the ullage. The ullage pressure is always known a priori, and the partial pressure of oxygen is equal to the saturation pressure at the bulk propellant temperature. It is recognized that the hydrostatic pressure from the liquid propellant is present upon bubbles as they exit the submerged diffuser, however, this does not directly affect the bulk temperature of the liquid propellant, and therefore does not change the oxygen partial pressure of the bubbles. GFSSP's Tank Pressurization option, which is utilized in the current work, tracks the hydrostatic pressure as the liquid propellant volume changes. Two cases were simulated, one using Equation 3 as written, and the other including the hydrostatic pressure on the left-hand-side of Equation 3. The two cases were otherwise identical. These cases serve to bound the solution, as they simulate the minimum and maximum pressures experienced by the bubbles as they travel through the liquid. The difference in the subcooling and oxygen evaporation data between the two runs was found to be less than one ten-thousandth of a percent at any given time step. Based on this comparison, it is assumed that the hydrostatic pressure has a nominal effect on the model results and that Equation 3 as written is sufficient. For clarity, the hydrostatic pressure is considered by GFSSP when solving the conservation equations; it is only omitted in the user-defined mass transfer equations. The rate of liquid propellant evaporation and diffusion is determined by the ideal gas law equation of state of the bubble, which can be assumed at temperatures and pressures below the gas critical point: The rate of liquid propellant evaporation and diffusion is determined by the equation of state of the bubble:

$$\dot{m}_{\mathrm{He}} = \frac{P_{\mathrm{He}}\dot{V}}{R_{\mathrm{He}}T_{\mathrm{He}}} \tag{4}$$

$$\dot{m}_{\mathrm{O_2}} = \frac{P_{\mathrm{O_2}}\dot{V}}{R_{\mathrm{O_2}}T_{\mathrm{O_2}}} \tag{5}$$

Dividing these equations results in the equilibrium model mass transfer equation:

$$\dot{m}_{\mathrm{O_2}} = \frac{P_{\mathrm{O_2}}R_{\mathrm{He}}}{P_{\mathrm{He}}R_{\mathrm{O_2}}}\dot{m}_{\mathrm{He}} \tag{6}$$

Evidently, the mass transfer rate is driven by the helium injection rate, ullage pressure, and liquid propellant temperature.

The terms in the mass and energy conservation equations for both the liquid propellant and ullage nodes are now discussed. For the liquid propellant node, the transient mass conservation equation and the enthalpy-based energy equation are given by:

$$m^{t}_{\mathrm{LOx}} - m^{t-\Delta t}_{\mathrm{LOx}} = -\left(\dot{m}_{\mathrm{O_2}} + \dot{m}_{\mathrm{ev}}\right)\Delta t - \dot{m}_{\mathrm{drain}}\Delta t \tag{7}$$

$$\frac{\left[m\left(h-\frac{P}{\rho}\right)\right]^{t}_{\mathrm{LOx}} - \left[m\left(h-\frac{P}{\rho}\right)\right]^{t-\Delta t}_{\mathrm{LOx}}}{\Delta t} = \dot{m}_{\mathrm{He}} C_{\mathrm{P,He}}\left(T_{\mathrm{He,in}} - T^{t}_{\mathrm{prp}}\right) - \left(\dot{m}_{\mathrm{O_2}} + \dot{m}_{\mathrm{ev}}\right)h_{\mathrm{g,O_2}} - \dot{m}_{\mathrm{drain}}h^{t}_{\mathrm{LOx}} + \dot{Q}_{\mathrm{leak}} + \dot{Q} + \left(\frac{P\Delta V}{\Delta t} + \frac{V\Delta P}{\Delta t}\right) \tag{8}$$

The first term on the right-hand-side represents both components of oxygen evaporation that take place: the mass transfer due to the liquid-ullage heat transfer (Equation 1), and the diffusional mass transfer induced by the

concentration gradient (Equation 6). This evaporated oxygen leaves the liquid propellant node and enters the ullage node at each time step. GFSSP employs a mass sink and a species concentration sink in the liquid propellant node to account for this evaporation, balanced with a mass source and a species concentration source in the ullage node (In multi-fluid models, GFSSP has a separate species concentration equation that needs to be solved in addition to the mass and energy equations). It is noted that the current model assumes that the rate of helium entering the liquid propellant node is equal to the amount of helium entering the ullage node, resulting in a net zero change in helium mass. The final term on the right-hand-side of Equation 7 is omitted if the propellant does not drain.

The left-hand-side of Equation 8 is the change in internal energy of the liquid propellant node. As mentioned above, the first term on the right-hand-side is the enthalpy change that results from the heat exchange from the warm helium to the surrounding liquid. The second term on the right-hand-side is the energy required to vaporize the liquid propellant during the mass transfer process. Thermal energy from the liquid is used to cause the phase change. The third term on the right is the enthalpy leaving the tank as it drains. Terms four and five represent the heat leak into the liquid propellant and the heat transfer from the ullage to the liquid propellant, respectively. Finally, the last term on the right-hand-side represents the positive work done by the ullage on the liquid due to the effects of tank drain, evaporation, boil-off, and pressurization. In a no-drain case, this term is negligible, and the drain term is removed. All these energy terms are represented as enthalpy sources and sinks in the GFSSP user subroutine.

For the ullage node, the corresponding equations are given below by:

$$m_{\mathrm{u}}^{t} - m_{\mathrm{u}}^{t-\Delta t} = \left(\dot{m}_{\mathrm{O_2}} + \dot{m}_{\mathrm{ev}} + \dot{m}_{\mathrm{He}} - \dot{m}_{\mathrm{vent}}\right)\Delta t \tag{9}$$

$$\frac{\left[m\left(h-\frac{P}{\rho}\right)\right]_{\mathrm{u}}^{t} - \left[m\left(h-\frac{P}{\rho}\right)\right]_{\mathrm{u}}^{t-\Delta t}}{\Delta t} = \left(\dot{m}_{\mathrm{O_2}} + \dot{m}_{\mathrm{ev}}\right)h_{\mathrm{g,O_2}} + \dot{m}_{\mathrm{He}}h_{\mathrm{He}} - \dot{m}_{\mathrm{vent}}h_{\mathrm{u}} + \dot{Q}_{\mathrm{leak}} - \dot{Q} - \left(\frac{P\Delta V}{\Delta t} + \frac{V\Delta P}{\Delta t}\right) \tag{10}$$

In Equation 9, the term on the right includes both components of oxygen mass transfer entering the ullage, the helium pressurant entering the ullage, and the ullage gases being vented from the ullage. The left-hand-side of Equation 10 is the change in internal energy of the ullage node. The first term on the right is the energy required to vaporize the liquid propellant during the mass transfer process. The second term is the helium enthalpy entering the ullage, and the third term is the enthalpy of the ullage gases being vented from the tank. The other terms are identical to those discussed above for the liquid propellant node. The venting terms in both equations are omitted if the ullage gases are not vented. All these energy terms are represented as enthalpy sources and sinks in the GFSSP user subroutine.

III. Experimental Apparatus

A. Cho et al.

The experimental work of Cho et al. [1-2] investigated the propellant subcooling effect as a function of system pressure, helium injection temperature, and helium injection flowrate for a no-drain submerged injection system. The apparatus consisted of one of two vacuum and multi-layer insulation (MLI) insulated liquid oxygen Dewars with varying geometry. The volumes of the Dewars were given as 90 liters and 60 liters with diameters 0.23 meters and 0.2 meters respectively. An illustration of both Dewars is shown in Figure 1. One Dewar contained a helium cooling unit to investigate the effect of pressurant temperature on propellant subcooling. The tests consisted of injecting helium of various conditions and flowrates beneath the liquid oxygen surface and

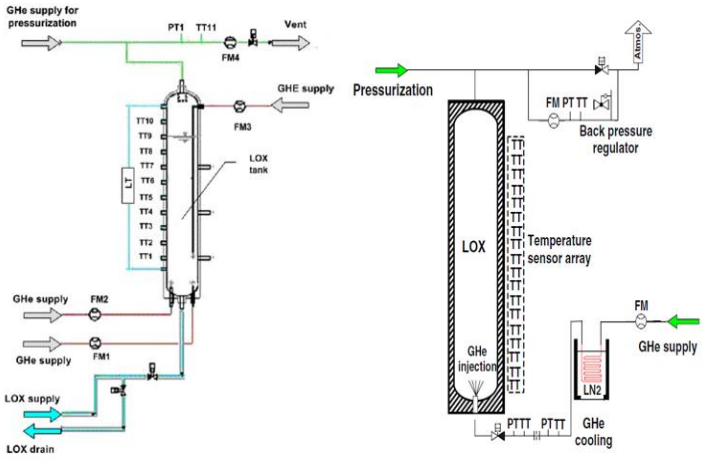

Figure 1: Depiction of the experimental apparatus of Cho et al. [1-2]; Left: Room temperature injected helium; Right: Sub-room temperature injected helium.

recording the temperatures as a function of time. For the tests considered, the helium was injected through a single diffuser in an upward direction. A series of wetted platinum resistance temperature detectors (RTDs) was placed axially along the Dewar to measure temperature, and the system pressure was held constant via ullage venting. A constant heat leak value for each case was provided and assumed to be distributed evenly throughout the entire Dewar volume. No experimental uncertainty was reported for these tests.

B. Centaur Test Vehicle

The data from the Centaur test cases were obtained at the High Energy Rocket Research Facility located at the Lewis Research Center [4-5]. The purpose of these ground tests was to assess the feasibility of replacing the Centaur's boost pump system with a gas pressurization system. The test cases for the Centaur test vehicle included pre-pressurization (ramp), direct ullage injection, and submerged injection data. The 9.78 cubic meter stainless steel oxygen tank comprises two spheroidal halves separated by a cylindrical portion 0.11 meters in height. The spheroidal components have a major and minor axis of 3.02 meters and 2.2 meter, respectfully. The tank walls located above the cylindrical element are thermally insulated, and a heat leak of 5.9 kilowatts into the tank is assumed to only occur on the bottom half of the tank, according to the report. For the submerged injection cases, the helium injector inlet was located below 91.5% of the tank volume. A series of platinum RTDs was placed axially along the tank to measure temperature. No experimental uncertainty was reported for these tests. A schematic of the oxygen tank can be seen in Figure 2.

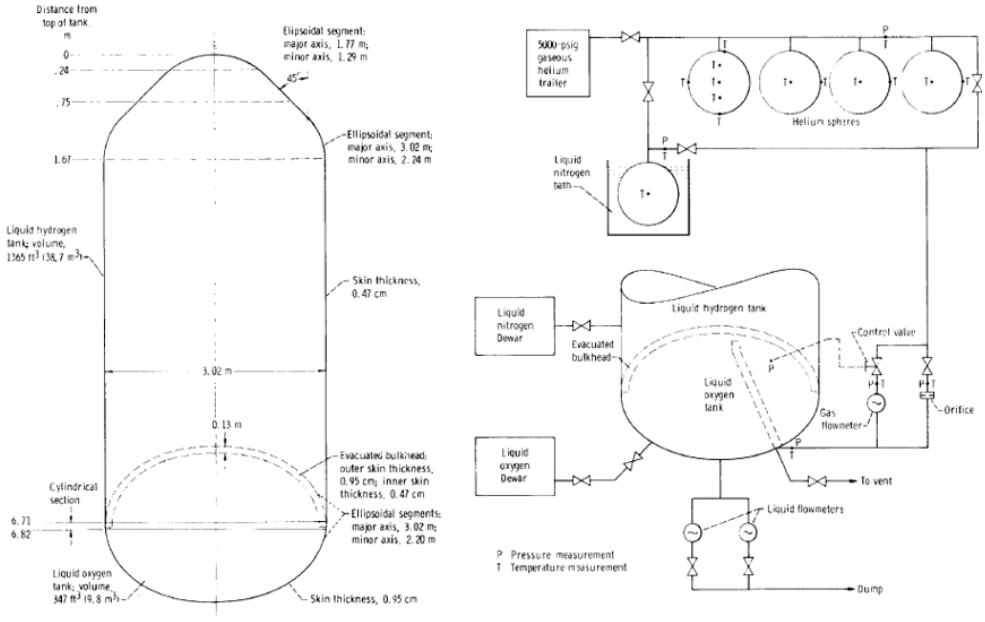

Figure 2: Depiction of the Centaur test vehicle liquid oxygen tank [4].

The pre-pressurization cases consisted of a ramp phase and a hold phase. In the ramp phase, helium pressurant was directly injected into the ullage until a target ullage pressure was achieved. The time to reach said ullage pressure varied from one second to 75 seconds. Next is the hold phase, where a small amount of propellant would drain from the tank to precondition the engine feedline while maintaining a constant ullage pressure. The hold time was either 15 seconds or 60 seconds.

The direct ullage and submerged injection cases follow the same experimental procedure, the sole difference being where the helium pressurant is injected. Each test contained a one second ramp phase, a 15 second hold phase, and a drain phase that lasted several hundred seconds. The ramp and hold phases were done identically as described above. Once the hold time had elapsed, a target propellant drain rate of 25.6 kilograms per second was maintained by controlling the ullage pressure via helium injection.

For the direct ullage injection cases (including the pre-pressurization cases), the helium entered the oxygen tank through a tube located in the lower right quadrant as seen in the right diagram of Figure 2. The tube extended through the liquid, and the helium was injected into the ullage towards the top of the tank. For each test case, the Centaur report provides the average helium temperature into the bottom of the tank but not the temperature injected into the ullage. These data are available for only two of the pre-pressurization cases and two of the direct ullage injection pressurization cases and are shown below in Figures 3 and 4. Clearly the heat transfer from the helium to the liquid propellant through the supply tube is significant, and the GFSSP modeling of the inlet helium temperature into the ullage will be discussed later.

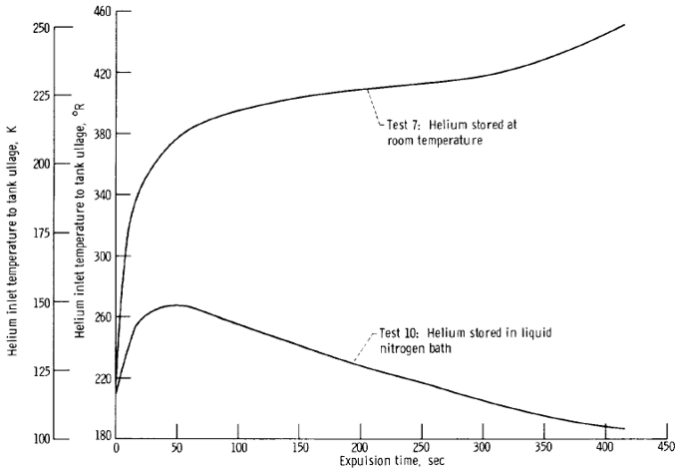

Figure 4: Temporal helium injection temperatures for direct ullage pressurization cases 7 and 10 [4].

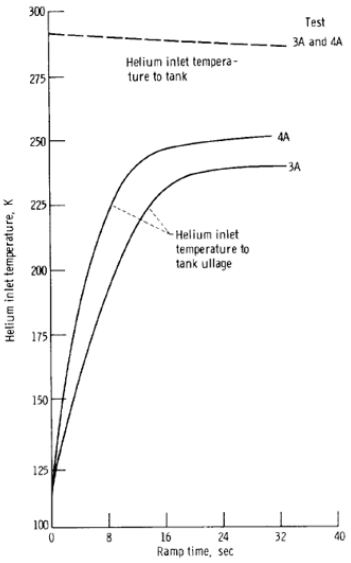

Figure 3: Temporal helium injection temperatures for pre-pressurization cases 3A and 4A.

IV. GFSSP Model

A. Cho et al.

Figure 5 shows the GFSSP model of the experimental Dewars described in the Cho et al. [1-2] papers. The model utilizes the advanced Tank Pressurization option and is divided into two parts. The ullage node (node 2) is connected to an ambient reservoir (node 1), both set to the specified system pressure. As helium is injected into the liquid, the ullage experiences an increase in pressure as both helium and gaseous propellant enter it. The pressure differential between nodes 1 and 2 results in the flow of the ullage gases out of the ullage through branch 21, such that the target system pressure is maintained. This set of experiments specified a constant helium injection rate; this value, along with the helium inlet temperature and pressure, is hard coded in the user subroutine.

The bottom part of the model contains the liquid oxygen propellant node (node 4). The so-called pseudo-boundary node (node 3) is responsible for the thermodynamic continuity between the ullage and liquid propellant nodes and serves no physical purpose. The pseudo-boundary node separates the gaseous ullage node from the liquid propellant node, which would otherwise mix homogeneously if connected by a branch. Branch 34 can be thought of as the ullage-liquid interface. The Dewar itself is modeled as a cylinder.

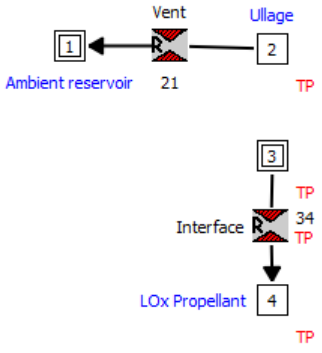

Figure 5: GFSSP canvas model of the Cho et al. [1-2] oxygen Dewar venting system.

The mass and energy equations are modified in the user subroutine. Since the initial ullage pressure and helium injection rate are known, Equations 1-6 are closed and can be solved. The experimental apparatus does not contain a propellant drain line, so the liquid propellant mass and energy equations are modified to take the following form:

$$m_{\mathrm{LOx}}^{t} - m_{\mathrm{LOx}}^{t-\Delta t} = -\left(\dot{m}_{\mathrm{O_2}} + \dot{m}_{\mathrm{ev}}\right)\Delta t \tag{11}$$

$$\frac{\left[m\left(h-\frac{P}{\rho}\right)\right]_{\mathrm{LOx}}^{t} - \left[m\left(h-\frac{P}{\rho}\right)\right]_{\mathrm{LOx}}^{t-\Delta t}}{\Delta t} = \dot{m}_{\mathrm{He}} C_{\mathrm{P,He}}\left(T_{\mathrm{He,in}} - T_{\mathrm{prp}}^{t}\right) - \left(\dot{m}_{\mathrm{O_2}} + \dot{m}_{\mathrm{ev}}\right) h_{\mathrm{g,O_2}} + \dot{Q}_{\mathrm{leak}} + \dot{Q} \tag{12}$$

The appropriate liquid propellant and ullage source and sink terms are then applied in the user subroutine.

B. Centaur Test Vehicle

Figure 6 shows the direct ullage injection and submerged injection GFSSP models of the oxygen tank for the investigated Centaur test vehicle [4]. The models utilize the Tank Pressurization option and is divided into two parts as discussed earlier. The ullage and liquid propellant nodes are represented by node 1 and node 3 respectively, and branch 34 is the propellant draining outlet to the engine feedline. Pseudo-boundary node 2 and branch 23 serve the same purpose as their counterparts in the Cho et al. [1-2] work. In contrast to the Cho et al. [1-2] work, the Centaur test vehicle ullage pressure is maintained by the helium injection rate. The oxygen tank geometry is modeled using the customizable tank feature within the GFSSP advanced Tank Pressurization option. This allows the user to specify tank volume, wall surface area, and liquid propellant surface area as functions of tank depth using interpolation tables. Ullage-to-wall and ullage-to-liquid heat transfer are handled by the Tank Pressurization option using standard flat plate natural convection correlations. The user has the ability to apply an adjustment factor to the calculated heat transfer coefficient.

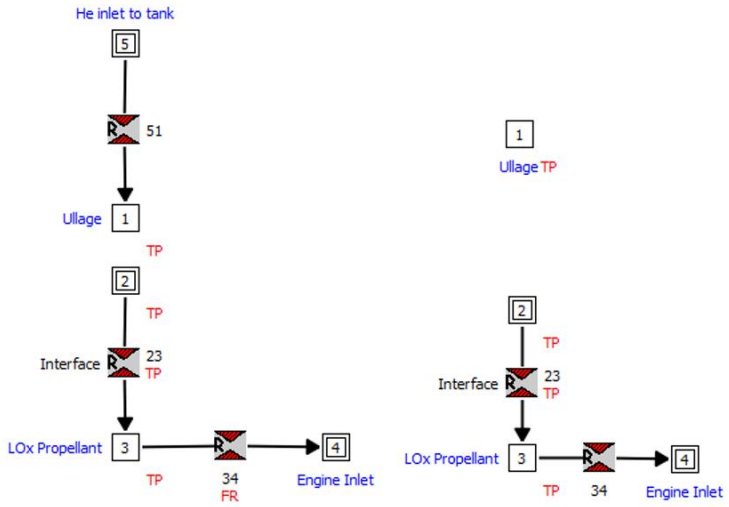

Figure 6: GFSSP canvas model of the Centaur test vehicle system; Left: direct ullage injection; Right: submerged injection.

The direct ullage injection model contains an additional boundary node and branch connecting said boundary node to the ullage node. These represent the helium inlet conditions and flow into the tank ullage, respectively. The incoming helium maintains the ullage at its target pressure. As discussed earlier, the Centaur report only provides the average helium injection temperature into the bottom of the oxygen tank. The actual temperature entering the ullage is much colder, as the helium undergoes substantial cooling as it travels through a tube surrounded by liquid oxygen propellant. The only available data regarding the helium injection temperature into the ullage is provided in Figures 3 (ramp tests) and 4 (direct ullage pressurization tests). For these four cases, the graphical data from the Centaur report were digitized and used in node 5 as boundary conditions. For the remaining cases, the temperature curves were estimated by vertically shifting the provided curves by the difference in the average tank inlet values given for each case. For the pre-pressurization cases, test cases 4A, 4B, and 4C utilized the case 4A curve in Figure 3; the remainder of the test cases used the case 3A curve. The only practical experimental difference between cases 3A and 4A was the target ramp pressure; therefore, since only two target ramp pressures were tested, the helium injection curves were divided by ramp pressure. It is acknowledged that this estimation introduces modeling uncertainty, but with the data available no other suitable alternative was thought to be superior. The same process was followed for the direct ullage pressurization cases. Case 10 in Figure 4 shows the only test where the helium was highly cooled. All other cases used the case 7 temperature curve as a reference point.

For the submerged injection model, the helium inlet temperature and pressure are hard coded in the user subroutine. This is necessary because injecting helium beneath the surface is accompanied by the diffusion mass transfer of oxygen. As a result, maintaining the target ullage pressure is more involved and must be determined iteratively.

The mass and energy equations are modified in the user subroutine. The direct ullage injection user subroutine contains no diffusion mass transfer and consists of boil-off evaporation (Equation 1) and a set of customized heat leak equations specific to the Centaur test vehicle. The appropriate ullage and liquid propellant heat sink and source terms in Equations 7-10 are applied. In the submerged ullage user subroutine, an initial guess for the helium flowrate is made, and Equations 1-10 are iteratively solved until the target ullage pressure is resulted.

V. Results and Discussion

A. Cho et al.

Table 1 shows the various test case parameters simulated. The labeling of the test cases is presented here for simplicity and are not labeled as such in the original papers. Results are seen in Table 2 and plots for each test case immediately follow. The propellant subcooling is defined as

$$\Delta T_{\text{sub}} = T_{\text{initial}} - T_{\text{final}} \tag{13}$$

and the error between the experimental and simulated subcooling data was computed using the following definition:

$$\varepsilon_{\text{sub}} = \frac{\Delta T_{\text{sub,sim}} - \Delta T_{\text{sub,exp}}}{\Delta T_{\text{sub,exp}}} \tag{14}$$

where 'sim' and 'exp' represent the simulated and experiment results, respectively. Positive error values indicate that the simulations overpredicted the propellant subcooling. Ullage-to-wall and ullage-to-liquid heat transfer are handled by the Tank Pressurization option using standard flat plate natural convection correlations suggested by [6]. The user

Table 1: System parameters for the Cho et al. [1-2] test cases

Test Case	Initial Fill Volume, L	Initial Ullage Volume, L	System Pressure, bar	Initial LOx Temperature, K	Ambient Heating Rate, W	Helium Injection Rate, g/s	Helium Injection Temperature, K
1	65.0	25.0	1	90.8	261	0.38	288
2	65.0	25.0	1	90.8	261	0.25	288
3	65.1	24.9	1	90.9	261	0.16	288
4	72.0	18.0	3	101.8	150	0.82	288
5	48.0	12.0	3.5	98.9	175	1.55	114
6	72.0	18.0	1	91.2	150	0.21	288
7	48.0	12.0	1	90.2	175	0.14	140
8	48.0	12.0	1	90.2	175	0.46	114
9	72.0	18.0	3	91.0	150	0.74	288
10	72.0	18.0	3	91.4	150	0.49	288

Table 1: Results for the Cho et al. [1-2] test cases

Test Case	Experimental Time, s	$\Delta T_{sub,exp}$, K	$\Delta T_{sub,sim}$, K	$\Delta T_{sub,sim} - \Delta T_{sub,exp}$, K	ε_{sub} ,%
1	1600	5.4	6.3	0.9	16.7
2	1600	4.7	5.5	0.8	17.0
3	1600	4.3	4.5	0.2	4.7
4	1400	7.8	9.3	1.5	19.2
5	1400	12.0	13.3	1.3	10.8
6	600	4.0	3.9	-0.1	-2.5
7	600	4.6	3.4	-1.2	-26.1
8	600	6.8	6.6	-0.2	-2.9
9	1400	-1.9	-0.7	1.2	-63.2
10	1400	-2.0	-0.6	1.4	-70.0

can apply an adjustment factor to the calculated heat transfer coefficient, but for these simulations, the default coefficients are used.

Figure 7 shows the subcooling dependence on the room-temperature helium injection rate at atmospheric pressure. As expected, the subcooling increases as the helium injection rate increases. The increased presence of helium presents more volume where oxygen mass diffusion can occur. The GFSSP simulations overpredict the subcooling in all three cases, with 17.0% being the largest difference. The final liquid propellant temperature predictions are within one Kelvin cooler in all cases. This overprediction is a direct consequence of the instantaneous modeling assumptions where mass transfer is optimal and heat transfer is simplified. For a constant ullage pressure and helium injection flowrate, Equation 6 shows that the mass diffusion rate is greater at larger oxygen partial pressures in the bubble. Since the oxygen partial pressure is taken to be the saturation pressure at the liquid temperature, it is largest at the beginning of the run, when the liquid propellant temperature is highest. Since propellant subcooling immediately occurs because of mass transfer, the oxygen partial pressure only decreases with time. The steep initial liquid propellent temperature slopes for the simulated cases imply larger diffusion rates. The test data show smaller slopes, indicating less initial mass transfer than the ideal model predicts.

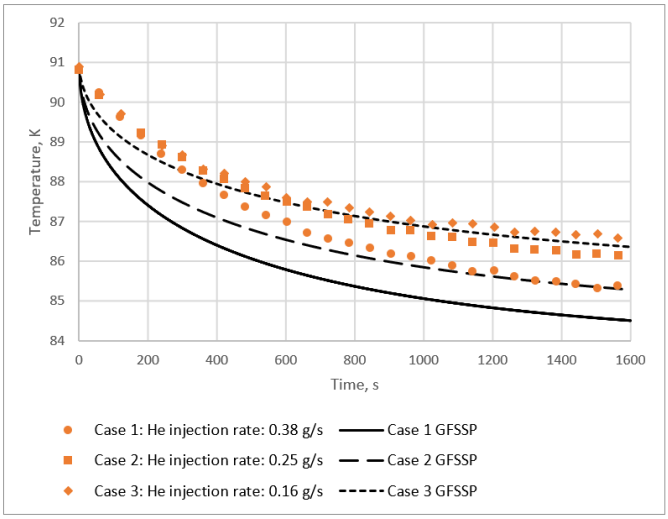

Figure 7: Subcooling dependance on room-temperature helium injection rate at liquid propellant saturation conditions (atmospheric pressure).

Figure 8 shows the experimental and simulated predictions for two cases conducted at elevated pressures. Case 4 features room temperature helium while case 5 injects 114 K helium at almost double the flowrate. The results qualitatively resemble those presented above in Figure 7 with the higher helium injection rate case resulting in greater subcooling, and with more rapid subcooling being seen towards the beginning on the test. GFSSP overpredicts the Case 4 subcooling by 18.6%. The final liquid propellant temperature predictions are within 1.5 Kelvin cooler in both cases.

Figure 9 displays the results for injected atmospheric helium at various flowrates and temperatures. By virtue of differing flowrates, it is difficult to ascertain the effect of the helium temperature on the propellant subcooling. As in the previous figures, greater subcooling is observed at greater helium injection rates for the simulated cases. It should be noted that Case 6 has a larger simulated subcooling than Case 7 owing to the initial condition of the liquid. However, the test data show that the subcooling is greater for Case 7 despite the slower injection rate. This suggests that the lower helium injection temperatures enhance subcooling. By inspection and conjecture, it appears that the effects of helium temperature and helium injection rate on propellant subcooling are of similar importance.

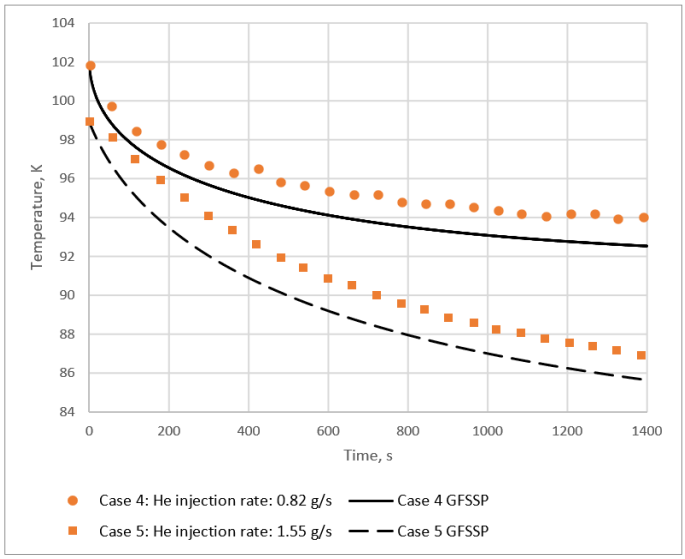

Figure 8: Subcooling at liquid propellant saturation conditions (elevated pressure).

This discrepancy between the case 6 and case 7 results has at least a couple of possible explanations. The first is that the assumptions of the instantaneous heat and mass transfer model fail to appropriately simulate the particle interaction within the bubble at varying injection temperatures, leading to systematic modeling error. In the model implemented in the current work, the temperature of the helium is only considered as a heat source to the liquid propellant, which counteracts the effect of mass diffusion subcooling. However, warmer liquid has a higher oxygen saturation pressure, and by extension a higher oxygen partial pressure in the bubble. This serves to increase the diffusional mass transfer, since only the partial pressure of oxygen is directly considered in the mathematical formulation (see Equation 6). These processes oppose each other, and the dominant one will determine the subcooling dependence on helium temperature. In this particular case, the helium effects on mass transfer dominate the heat transfer. As a result, the model predicts that warmer helium results in greater subcooling. On the other hand, finite heat and mass transfer models monitor the thermodynamic state of the bubble more closely, and an increase in the liquid propellant saturation temperature also increases the oxygen partial pressure in the bubble, both of which are considered. This pressure gradient is what drives the mass transfer, so an increase in both pressures limits the magnitude of mass transfer. This is a possible explanation as to why the lower temperature test data resulted in larger subcooling.

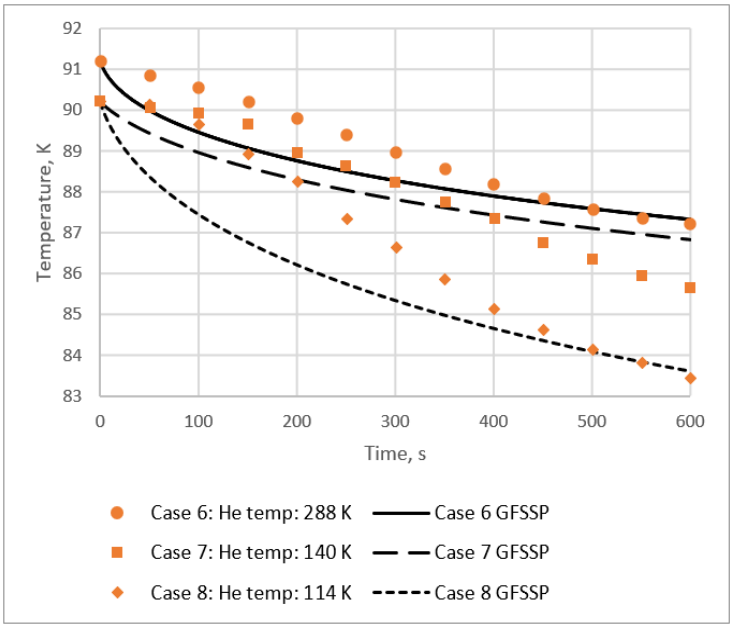

Figure 9: Subcooling dependance on helium injection temperature at liquid propellant saturation conditions

The second explanation is experimental uncertainty and/or experimental systematic error associated with the case 6, case 7, and case 8 test series. It is observed that in the previous five cases, the test data decreased in a way similar to the simulated predictions, with a positive concavity for the entirety of the test. This is clearly not true in the three

cases considered here. All these cases demonstrate a negative concavity for the first half of the test, approximately, followed by a positive concavity for the second half. Case 6 was conducted with room temperature helium, identical to the first five cases, so it is expected that the results would follow a similar qualitative shape. Furthermore, case 5 above was conducted with helium at 114 K, and those results do not show an obvious concavity shift. Finally, it is recalled that this experiment contained two apparatus: one for room temperature helium, and one for cooled helium. Case 6 evidently used a different apparatus than cases 7 and 8, but the concavity shift is still present. Also, as noted earlier, case 5 was conducted in the second apparatus, but no noticeable concavity shift was seen. From these observations, it is concluded that during this series of test cases, an unaccounted for experimental systematic error may have existed.

B. Centaur Test Vehicle

1) Ramp Pre-Pressurization Test Cases

Table 3 shows the various ramp test case parameters. Tables 4 and 5 display the simulated results when using default and tripled ullage-to-wall and ullage-to-liquid GFSSP heat transfer coefficients, respectively. The choice to triple the heat transfer coefficient was an arbitrary one; its purpose is to show the effect of the ullage heat transfer on the helium consumption and liquid propellant vaporization. The error between the experimental and simulated helium consumption data was computed using the following definition:

$$\varepsilon_{\text{cons}} = \frac{m_{\text{cons,sim}} - m_{\text{cons,exp}}}{m_{\text{cons,exp}}} \tag{15}$$

where 'sim' and 'exp' represent the simulated and experiment results, respectively. Positive error values indicate that the simulations overpredicted the helium consumption.

Table3: System parameters for the Centaur test vehicle [4] ramp cases

Test Case	Initial Fill Volume, m^3	Initial Ullage Volume, m^3	Initial Ullage Pressure, kPa	Ramp Ullage Pressure, kPa	Ramp Time, s	Hold Time, s	Outflow During Hold, kg/s	Ambient Heating Rate, kW	Average Tank Inlet Helium Temperature, K
1A	1.18	8.6	173	263	28	60	3.6	5.9	289
1B	1.18	8.6	173	263	39	60	3.6	5.9	283
1C	1.18	8.6	173	263	59	60	3.6	5.9	277
2A	3.98	5.8	173	263	25	60	0	5.9	283
2B	3.98	5.8	173	263	25	60	0	5.9	286
3A	4.08	5.7	173	263	33	60	3.6	5.9	289
3B	3.98	5.8	173	263	25	60	3.6	5.9	289
4A	4.08	5.7	173	310	31	60	3.6	5.9	289
4B	4.08	5.7	173	310	45	60	3.6	5.9	284
4C	4.08	5.7	173	310	75	60	3.6	5.9	277
5A	6.88	2.9	173	261	10	60	3.6	5.9	289
5B	6.88	2.9	173	261	14	60	3.6	5.9	292
6A	9.48	0.3	173	259	1	15	3.6	5.9	292

Table 4: Results for the Centaur test vehicle [4] ramp cases with default GFSSP ullage-to-liquid and ullage-to-wall heat transfer coefficients.

Test Case	Experimental Helium Usage, kg	Simulated Helium Usage, kg	Percent Difference, %	Simulated LOx evaporated, kg
1A	2.11	1.70	-19.6	0.48
1B	2.05	1.73	-15.8	0.53
1C	2.09	1.77	-15.4	0.62
2A	1.52	1.21	-20.6	0.55
2B	1.54	1.21	-21.6	0.55
3A	1.81	1.03	-43.2	0.52
3B	1.84	1.02	-44.8	0.48
4A	2.42	1.41	-41.6	0.78
4B	2.43	1.45	-40.3	0.86
4C	2.43	1.55	-36.1	1.01
5A	1.07	0.78	-27.5	0.29
5B	1.07	0.76	-29.4	0.32
6A	0.14	0.09	-38.8	0.01

Table 5: Results for the Centaur test vehicle [4] ramp cases with tripled GFSSP ullage-to-liquid and ullage-to-wall heat transfer coefficients.

Test Case	Experimental Helium Usage, kg	Simulated Helium Usage, kg	Percent Difference, %	Simulated LOx evaporated, kg
1A	2.11	2.63	24.5	1.09
1B	2.05	2.67	30.3	1.15
1C	2.09	2.85	36.6	1.32
2A	1.52	1.74	14.6	1.22
2B	1.54	1.75	13.7	1.24
3A	1.81	1.46	-19.4	1.11
3B	1.84	1.41	-23.2	1.04
4A	2.42	2.00	-17.2	1.67
4B	2.43	2.07	-14.7	1.80
4C	2.43	2.20	-9.6	2.00
5A	1.07	1.00	-6.3	0.65
5B	1.07	0.99	-7.1	0.70
6A	0.14	0.10	-28.2	0.03

Figures 11-16 shows the results for the ramp tests for the Table 4 simulations. The results for Tables 5 are not presented here because they follow the same shapes as the results provided here; the pertinent differences being the amount of helium consumed during the process. Cases with longer ramp times required a lower helium injection rate to pressurize the tank. The results indicate that increasing the GFSSP heat transfer coefficient between the ullage and the liquid requires more helium. Heat being removed from the ullage at a faster rate results in an increased rate of ullage temperature and pressure drop. More helium is therefore needed to maintain the target ullage pressure. Cases 2A and 2B show the effect of helium injection temperature on the total helium usage, but due to the small difference in the temperatures, it is difficult to draw any definitive conclusions. Figure 12 illustrates the impact of the injection temperature on the ullage pressure. Both cases have virtually identical results.

Clearly the GFSSP ullage-to-wall and ullage-to-liquid heat transfer coefficients have a significant impact on the predicted helium usage and vaporized propellant. Tripling the heat transfer coefficients increases these predictions by factors of 1.5 and two and exhibit better agreement with the test data. As mentioned earlier, GFSSP uses standard flat plate natural convection heat transfer coefficients to model the heat exchange between ullage and tank wall as well

as ullage and liquid. As helium enters the ullage near the top of the tank, it flows along the tank walls. A more realistic representation of the heat transfer would include a forced convection component, which would serve to increase the predicted heat transfer. This explains why the default GFSSP correlations underpredict the helium consumption data in every test case considered. The Centaur test data do not include information on the amount of vaporized propellant, but it is reasonable to conclude that higher GFSSP ullage heat transfer coefficients will result in great amounts of vaporized propellant when compared with identical test cases using the default correlations. From this data set, the GFSSP model does not overpredict the helium usage when default heat transfer is applied. Under these conditions, the current model can be used to predict a lower limit of helium usage and propellant vaporized than is actually consumed. Tripling the heat transfer coefficients results in better than 30% agreement between the GFSSP predictions and the test data in most of the cases.

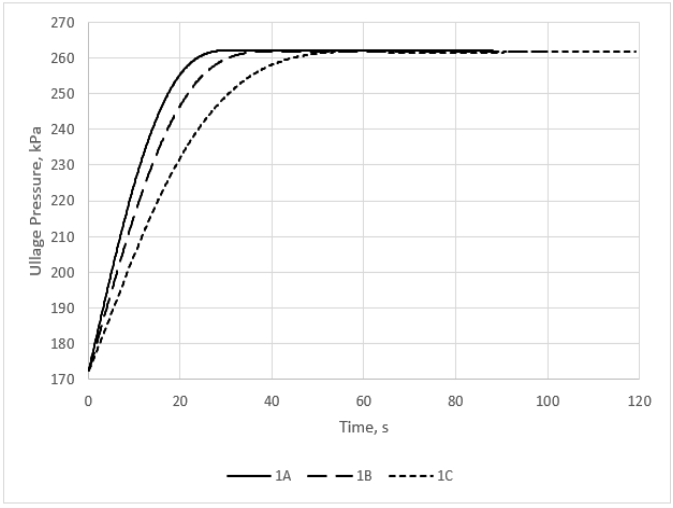

Figure 11: Predicted ullage pressure for Centaur ramp test series 1.

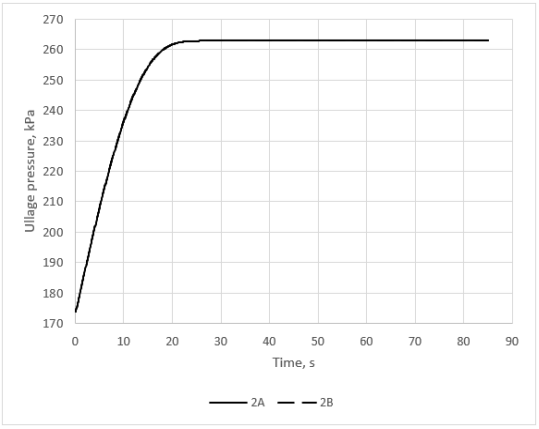

Figure 12: Predicted ullage pressure for Centaur ramp test series 2.

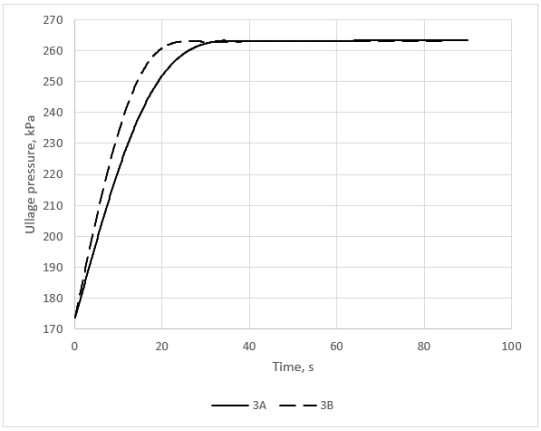

Figure 1: Predicted ullage pressure for Centaur ramp test series 3.

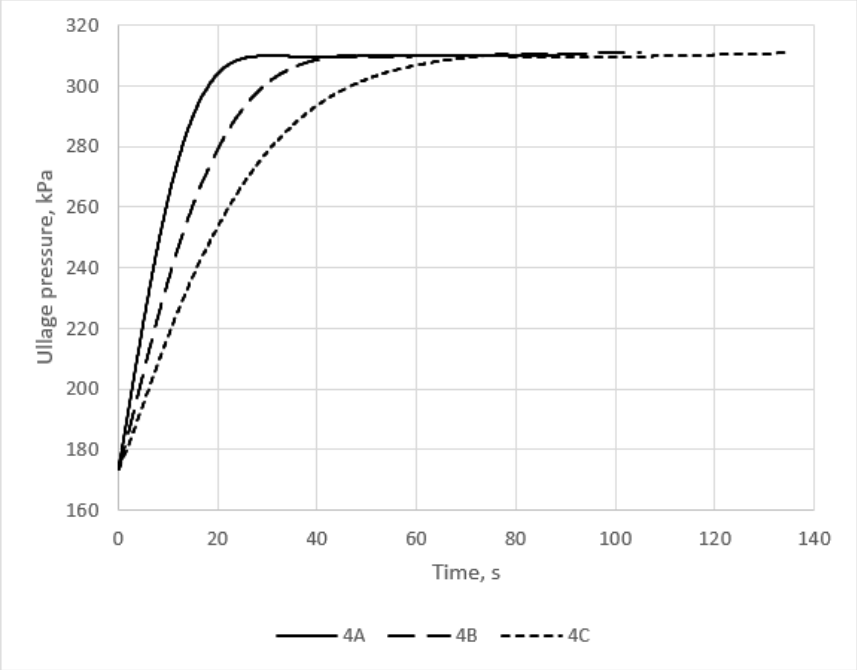

Figure 14: Predicted ullage pressure for Centaur ramp test series 4.

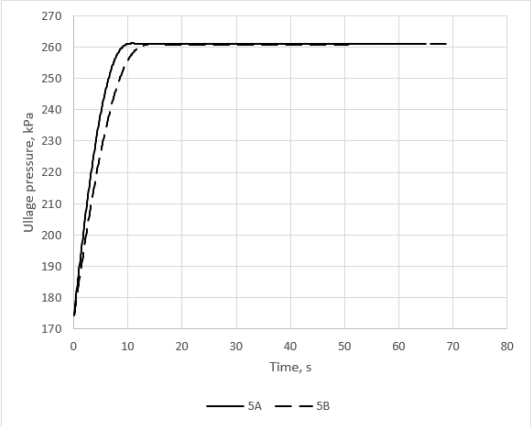

Figure 15: Predicted ullage pressure for Centaur ramp test series 5.

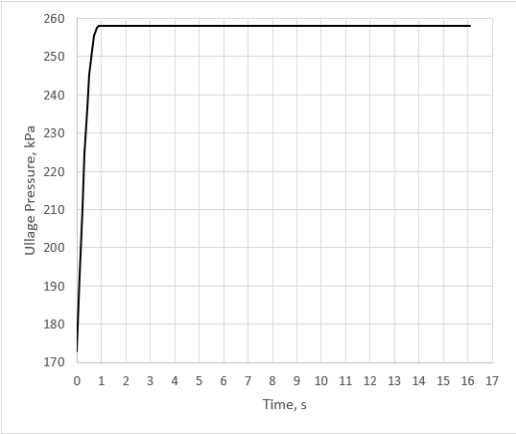

Figure 16: Predicted ullage pressure for Centaur ramp test 6.

2) Direct Ullage Injection Pressurization Test Cases

Table 6 shows the various direct ullage pressurization test case parameters. Tables 7 and 8 display the simulated results when using default and tripled ullage-to-wall and ullage-to-liquid GFSSP heat transfer coefficients,

respectively. The error between the experimental and simulated helium consumption data was computed according to Equation 15.

Table 6: System parameters for the Centaur test vehicle [4] direct ullage injection cases

Test Case	Initial Fill Volume, m^3	Initial Ullage Volume, m^3	Drain Ullage Pressure, kPa	Drain Time, s	Drain rate, kg/s	Ambient Heating Rate, kW	Average Tank Inlet Helium Temperature, K
7	9.48	0.3	244	415	25.6	5.9	278
8	9.48	0.3	244	415	25.6	5.9	279
9	9.48	0.3	276	415	25.6	5.9	275
10	9.48	0.3	244	415	25.6	5.9	142
11A	9.48	0.3	244	243	25.6	5.9	293
12A	9.48	0.3	244	368	25.6	5.9	290
13A	9.48	0.3	244	120	25.6	5.9	292
14A	9.48	0.3	276	242	25.6	5.9	291

Table 7: Results for the Centaur test vehicle [4] direct ullage injection cases with default GFSSP ullage-to-liquid and ullage-to-wall heat transfer coefficients.

Test Case	Experimental Helium Usage, kg	Simulated Helium Usage, kg	Percent Difference, %	Simulated LOx evaporated, kg
7	8.78	7.15	-18.6	3.10
8	8.64	7.14	-17.4	3.12
9	9.57	8.11	-15.3	3.33
10	10.37	9.58	-7.6	1.16
11A	4.89	4.11	-16.0	2.04
12A	7.10	6.24	-12.1	3.14
13A	2.94	1.94	-34.1	0.74
14A	5.11	4.60	-10.0	2.18

Table 8: Results for the Centaur test vehicle [4] direct ullage injection cases with triple the GFSSP ullage-to-liquid and ullage-to-wall heat transfer.

Test Case	Experimental Helium Usage, kg	Simulated Helium Usage, kg	Percent Difference, %	Simulated LOx evaporated, kg
7	8.78	8.29	-5.6	5.10
8	8.64	8.28	-4.3	5.14
9	9.57	9.37	-2.1	5.55
10	10.37	10.24	-1.2	1.86
11A	4.89	4.80	-2.0	3.46
12A	7.10	7.25	2.1	5.18
13A	2.94	2.29	-22.1	1.40
14A	5.11	5.37	5.1	3.75

Figures 17 and 18 show the liquid propellant temperature and helium injection rate results for three of the direct ullage injection test cases. The default GFSSP ullage-to-liquid heat transfer and distributed injection temperature configuration is displayed. The three selected cases were conducted under identical conditions, except for the helium injection temperature. As seen in Figure 17, the helium injection temperature has a nominal effect on the liquid

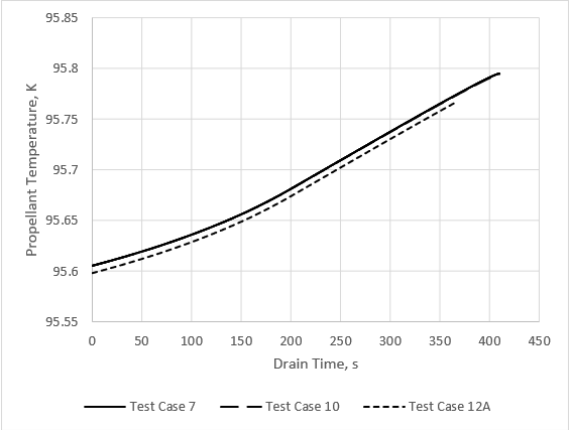

Figure 17: Liquid propellant temperatures for sample test cases at 244 kPa ullage pressure.

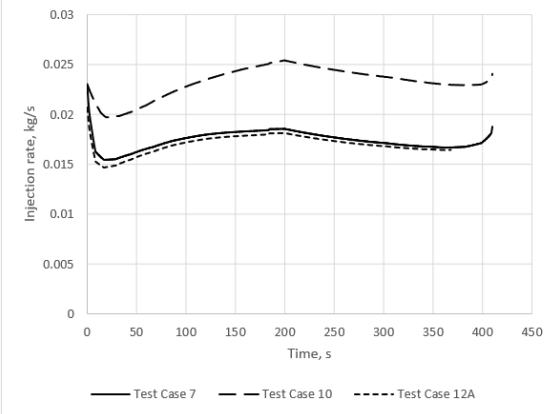

Figure 18: Helium injection rates for sample test cases at 244 kPa ullage pressure.

injected helium was significantly colder for the entire run, and its time-dependent injection temperature data is seen in Figure 4.

Similar to the ramp pressurization tests, GFSSP underpredicts the helium usage when using the default heat transfer coefficients. This further increases the confidence that the GFSSP model can be used to predict the helium usage lower bound. The majority of GFSSP default heat transfer predictions agree with the test data to within 20%; tripling the heat transfer coefficient reduces the discrepancy to below 6% in all but one case.

propellant temperature; however, it has a noticeable inverse relationship with the rate of injection. Colder helium directly injected into the ullage lowers the ullage pressure, and more helium is required to maintain the target pressure.

Figure 19 compares the helium injection rate for test cases 9 and 14A, where the ullage was held at a slightly higher steady state pressure. The results support the same conclusions drawn from the previous figure.

Figure 20 compares the case 7 results for the two various GFSSP heat transfer simulations reflected in Tables 7-8. Similar to the ramp test cases, the results indicate that increasing the GFSSP heat transfer coefficient between the ullage and the liquid requires more helium. The justification for this phenomenon is the same. Test case 10 is the only case where the

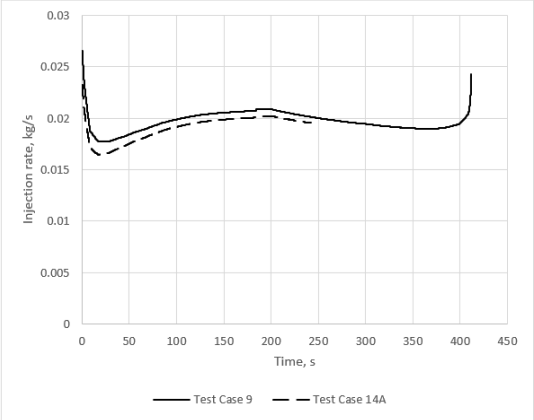

Figure 19: Helium injection rates for test cases at 276 kPa ullage pressure.

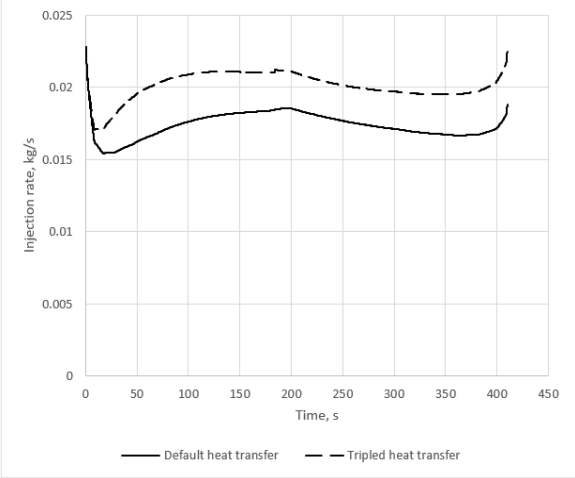

Figure 20: Helium injection rates for both ullage heat transfer variations for test case 7.

3) Submerged Injection Pressurization Test Cases

Table 9 shows the various submerged injection pressurization test case parameters. Table 10 displays the simulated results when using default ullage-to-wall and ullage-to-liquid GFSSP heat transfer coefficients. The error between the experimental and simulated helium consumption data was computed according to Equation 15.

Table 9: System parameters for the Centaur test vehicle [4] submerged injection cases

Test Case	Initial Fill Volume, m^3	Initial Ullage Volume, m^3	Initial Ullage Pressure, kPa	Drain Ullage Pressure, kPa	Drain Time, s	Drain rate, kg/s	Ambient Heating Rate, kW	Average Helium Injection Temperature, K
15	9.48	0.3	173	244	415	25.6	5.9	175
16	9.48	0.3	173	244	415	25.6	5.9	291
17	9.48	0.3	173	276	415	25.6	5.9	289
18	9.48	0.3	173	276	415	25.6	5.9	161
19A	9.48	0.3	173	244	243	25.6	5.9	195
20A	9.48	0.3	173	244	243	25.6	5.9	289
21A	9.48	0.3	173	222	243	25.6	5.9	289

Table 10: Results for the Centaur test vehicle [4] submerged injection cases with default GFSSP ullage-to-liquid heat transfer and distributed helium injection temperatures.

Test Case	Experimental Helium Usage, kg	Simulated Helium Usage, kg	Percent Difference, %	Simulated LOx evaporated, kg
15	4.38	3.74	-14.7	57.8
16	4.00	3.53	-11.8	58.3
17	5.50	4.89	-11.2	58.5
18	6.45	5.20	-19.3	57.9
19A	2.65	2.17	-18.3	40.2
20A	2.55	2.15	-15.7	40.3
21A	2.40	1.53	-36.4	40.1

Figure 21 compares the test data and simulated results for case 15 as well as a comparison to the case 16 simulated case with a higher helium injection temperature. The Centaur report contains time-dependent liquid propellant temperature data for case 15 only. Firstly, the subcooling test data agree well with the GFSSP instantaneous heat and mass transfer model predictions. Secondly, the results from the case 16 simulation indicate that lower helium injection temperatures result in increased

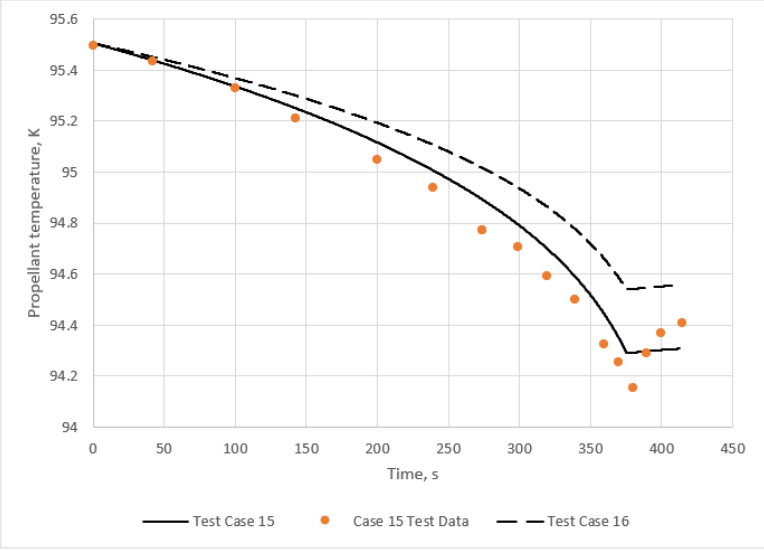

Figure 21: Propellant subcooling for submerged injection sample test cases.

propellant subcooling. This result supports the conclusion drawn in the Cho et al. [1-2] experiments; however, it should be noted that the helium injection rate is higher for case 15. Therefore, it is difficult to determine the extent to which the helium temperature impacts the propellant subcooling. The predicted helium consumption data agree with the test data to within 20% in all but one case.

VI. Conclusions

The instantaneous mass and heat transfer model implemented into GFSSP has been validated against two experimental sources and has shown to predict both propellant subcooling and helium consumption data to within 30% in most cases. These errors can be reduced by increasing the GFSSP ullage-to-liquid and ullage-to-wall heat transfer coefficients from their default values, which effectively adds a forced convective component to the ullage heat transfer. Pre-pressurization and direct ullage injection test data from the Centaur test vehicle were also included to increase confidence in the user-defined oxygen tank read in by GFSSP as well as to verify that GFSSP predictions of these processes are accurate. In almost all cases, the mass diffusion model overpredicted the propellant subcooling. This was the expected result in accordance with the idealized model.

The GFSSP results from the Cho et al. [1-2] experiments reaffirm that higher rates of helium injection enhance propellent subcooling. The impact of the injection temperature is less certain but appears to similarly affect both the heating and cooling of the liquid propellant (by enthalpy exchange and mass diffusion, respectively). The Centaur test cases show that submerged injection utilizes about half as much helium when compared to the direct ullage injection method at similar test environments. Furthermore, propellant subcooling is seen to be an additional benefit. Due to the lack of propellant subcooling data provided in the technical report, the relationship between helium injection temperature and propellant subcooling cannot be verified.

Based on the results of this work, the development of a finite heat and mass transfer model to simulate a submerged injection system is not necessary. The complexity of the physics and its associated uncertainties would serve to reduce the error by few percent. As indicated in these results, adjusting the ullage-to-liquid and ullage-to-wall heat transfer has a significant effect on the desired results, and the model can be improved by investigating the accuracy and fidelity of these correlations.

Based on the data sets investigated in this work, the following conclusions can be drawn regarding GFSSP as a predictive modeling tool for direct ullage and submerged tank pressurization systems:

1. Using the default GFSSP heat transfer correlations, the direct ullage injection cases underpredict the amount of helium required to pressurize the tank. Submerged injection cases at similar operating conditions require about half as much helium to pressurize. Increasing the GFSSP heat transfer coefficients for the direct ullage injection cases results in helium consumption predictions closer to that of the test data. This emphasizes the helium savings benefit that the submerged system offers. By comparing the two pressurization methods with default correlations, a conservative estimate for helium savings can be confidently determined.
2. Owing to the idealized mass diffusion model, the propellant subcooling present in the submerged systems are typically overestimated in GFSSP. The final liquid propellant temperatures are never found to deviate more than 3% of the test data. The results presented here show that GFSSP can predict the degree of subcooling well, and the prevention of liquid propellant heating offers practical advantages. The current model offers a slightly liberal estimate of the amount of subcooling that is to be expected.

This work supports the findings of previous studies that utilizing a submerged injection system for cryogenic tank pressurization delivers subcooled propellant to the engine and has the potential to reduce the weight of the pressurant system required to pressurize. The model implemented here assumes instantaneous heat and mass transfer and has been shown to predict the selected test data well. The heat transfer assumptions are best suited for systems in which the rising bubbles can achieve thermal equilibrium with the liquid; therefore, tanks that are designed to increase the bubble residence time are desired. Decreasing the difference between the liquid propellant and pressurant injection temperatures is another consideration. This would reduce the time required to reach thermal equilibrium. Diffuser designs that produce smaller diameter bubbles would accomplish the same goal and are recommended. The mass transfer assumptions are better for smaller diameter bubbles. This emphasizes the importance of the diffuser design if the numerical model developed here is to perform optimally. Finally, the mass transfer model is applicable to any gravitational environment, but important implications to the gravitational effect on submerged pressurization systems as a whole need to be considered. In low-g environments for example, the residence time of the bubbles in the propellant will be greatly increased, and bubbles may not reach the ullage due to the reduction of the buoyant force.

It is recommended that this phenomenon be investigated theoretically and experimentally to ensure the necessary conditions for pressurization are possible. In general, experiments and/or flight data on submerged injection systems in low-g environments should be conducted and/or investigated. Future work on the ullage effects from pressurant dissolution into the liquid propellant should also be investigated.

Acknowledgments

M. R. Baldwin thanks Mr. John Sharp and Mr. Daniel Hauser for their critical reviews of this work and Dr. Paul Schallhorn for providing useful references that greatly benefited this investigation.

References

[1] Cho, Namkyung, et al. "Investigation of helium injection cooling to liquid oxygen propellant chamber." *Cryogenics* 46.2-3 (2006): 132-142.

[2] Cho, Namkyung, et al. "Investigation of helium injection cooling to liquid oxygen under pressurized condition." *Cryogenics* 46.11 (2006): 778-793.

[3] Hansen, Hans C. "Technology Demonstration Mission (TDM) Cryogenic Fluid Management (CFM Portfolio Project: CFM Modeling Portfolio Plan." (2021)

[4] Lacovic, Raymond F.*Comparison of experimental and calculated helium requirements for pressurization of a centaur liquid oxygen tank*. No. E-5539. 1970.

[5] Johnson, William R. "Helium pressurant requirements for liquid-hydrogen expulsion using submerged gas injection." (1967).

[6] Lewis, J. D. "Rocket Propellant and Pressurization Systems. Edited by Elliot Ring. Prentice-Hall Inc., Englewood Cliffs, NJ, USA 1964. 310 pp. Illustrated. 78s." *The Aeronautical Journal* 68.648 (1964): 853-854.